Series-Wound Heteropolar Inductor Motor for Automotive Applications

David Meeker
QinetiQ North America
350 Second Ave.
Waltham, MA 02451 USA
Email: dmeeker@ieee.org

***Abstract*—This work considers a method of control for a heteropolar inductor motor for use in automotive applications. Previously, power factor for this type of machine was considered to be too low, and operation in the high-speed / constant-power region was not easily realized. To make the machine amenable to control with an automotive inverter and to eliminate the need for a separate field controller, the field winding is driven by a rectifier bridge attached in series to the phase windings. Motor currents are then prescribed by a novel vector control scheme that realizes high power factor over a wide range of operation.**

I. Introduction

Presently, the most widespread type of electric vehicle (EV) motor is an Interior Permanent Magnet (IPM) motor. This motor type has good power density, and the IPMs structure allows the motor to be operated in a constant-power flux weakening regime above the base speed (typically about 4000RPM) up to the motor's maximum speed (typically about 10,000RPM). However, permanent magnets are mechanically fragile, can be damaged by high temperatures, and have faced supply problems in the past. It is therefore desirable to have a motor that does not fundamentally depend on strong permanent magnets.

An alternative to IPM motors is the Induction Motor (IM), which has no permanent magnets. Induction motors are presently used by some electric vehicle vendors. The motors can be relatively power dense and can be readily operated with a reduced field above the motor's base speed. However, since high currents flow on the rotor, accommodation of rotor heating can be a design challenge. The power factor of an IM is also low relative to a PM machine.

Switched Reluctance Motors (SRMs) are also used in some automotive applications. The SRM has a very simple construction that is inexpensive to build relative to other motor designs. Since all current flows on the stator, the machine is also relatively easy to cool. However, SRMs have high torque ripple, and they are not very amenable to running in a field weakening mode.

Wound field heteropolar inductor machines [1]-[4] have some of the attributes of an SRM (i.e. simple rotor), but they are potentially easier to control with a voltage source inverter because of their relatively sinusoidal back electromotive force (implying lower torque ripple). This class of machines is typified by the Doubly Salient Synchronous Machine (DSSM)

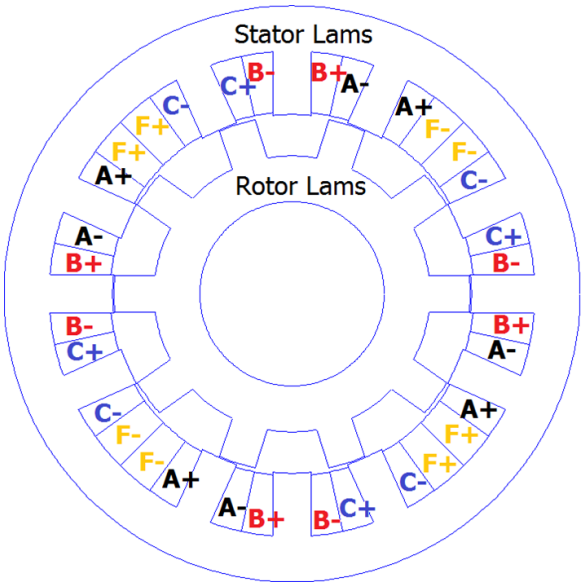

Fig. 1. Cross-section of a Doubly Salient Synchronous Machine.

described [3] and [4] and shown in Figure 1. The phase windings are arranged in four three-phase groups. Within each phase group, each phase winding is wound around a single stator tooth). A field winding wraps around all three teeth in each three-phase group (denoted in Figure 1 as the $F+$ and $F-$ windings). The teeth in adjacent three-phase groups are arranged to be out-of-phase, yielding a net bipolar flux linkage for each phase and canceling out even-numbered harmonics. However, heteropolar inductor machines have not been widely considered for automotive applications because they are viewed to have a very poor power factor. [5]

Here, a winding configuration and a method of control are proposed that enables heteropolar inductor motors to operate as high power density, non-permanent magnet electric drive systems suitable for use in electric vehicles or as general purpose servomotors. This control approach achieves a higher power factor than can be obtained by induction machines and permits straightforward operation into the field weakening region (above the machine's base speed) where the machine is simultaneously current and voltage limited. Since the machine is mechanically simple, it also realizes the advantages of

TABLE I
MACHINE PARAMETERS FOR EXAMPLE DSSM AND IM FROM [6].

Parameter	Units	DSSM	IM [6]
Pole Pairs		10 (effective)	2
Stator Teeth		12	48
Stator OD	mm	216	216
Stator Bore Dia.	mm	134.5	142
Stack Length	mm	170	170
Air Gap	mm	0.5	0.7
Number of Turns		7 (phase coils) 10 (field coils)	5
Copper fill factor		0.41 (phase) 0.45 (field)	0.4
End Connections (per side)	mm	35 (phase) 150 (field)	150
Max Speed	rpm	12,000	12,000
Continuous Torque @ 3.2kW loss	N*m	110	110
Speed at Cont. Torque	rpm	4000	4000
Current at Cont. Torque	A_{pk}	185	200
Current Density at Continuous Torque (in Cu cross-section)	$\frac{A_{rms}}{mm^2}$	10.1 (phase) 14.1 (field)	12 (est.)
Overload Torque	N*m	180	210
Overload Current	A_{pk}	360	360
Rated Phase Voltage	V_{pk}	173	173
Stator Resist. (130°C)	Ω	0.0222 (phase) 0.0495 (field)	0.027
Rotor Resist. (180°C)	Ω	N/A	0.018
Steel Grade		DI-MAX HF-10	M250-35A
Rotor Temperature	°C	150	150

a SRM with respect to robustness and potential low cost manufacture.

First, a representative machine and the proposed control approach are described. Predicted motor performance is then assessed versus an automotive induction motor design from the literature at the base and maximum speed operating points.

II. II. REPRESENTATIVE GEOMETRY AND MODEL

The proposed approach is meant to apply to heteropolar inductor motors. To examine the performance of the proposed approach, the parameters of a specific DSSM machine design (i.e. class of machine shown in Figure 1), sized for an electric vehicle application, are listed in Table 1. The parameters in Table 1 were selected to yield an EV motor whose performance is directly comparable to the IPM and IM designs considered in [6]. Specifically, the IM and DSSM designs have the same stator OD, stack length, and end turn length. Since the design continuous torque and speed is the same for both the IM and DSSM, the volume power density of these designs is the same. The machine has three-phase windings that carry AC current and DC field windings on the stator. In Table 1, it should be noted that the copper fill factor denotes the fraction of the bulk cross-section allocated for each coil (as shown in Figure 1) that is actually filled with copper. The rotor consists of a toothed stack of laminations with a 6o skew over the length of the rotor stack. Flux switching of the field produced by the DC field coil due to the spinning of the rotor produces a sinusoidal AC voltage in the phase coils.

A magnetic circuit analysis of this type of machine is

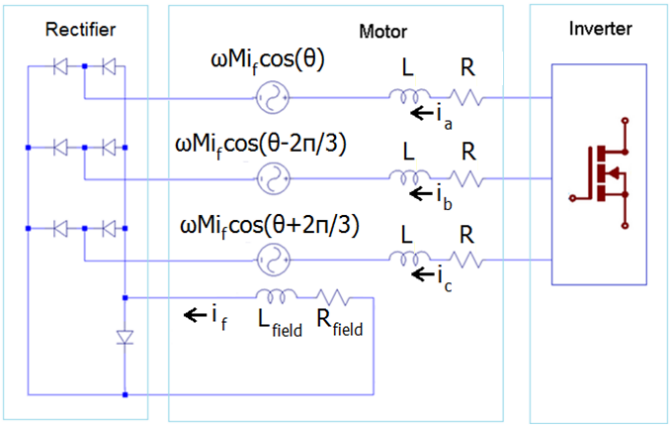

Fig. 2. Proposed configuration with field current obtained by rectifying the phase current.

presented in [4]. This analysis shows that the form of the machine's equivalent circuit model is the same that of a cylindrical rotor wound-field machine, as shown for example in [7]. Specifically, the steady-state, per-phase model of the machine is:

$$(j\omega L + R) = v - j\omega M i_f \tag{1}$$

where L and R are the phase inductance and resistance, respectively; M is the mutual inductance of the phase winding to the field winding; and i and i_f are the phase current (represented as a complex-valued phasor) and field currents, respectively.

For heteropolar inductor machines, it is desirable to use the same type of voltage source inverter that is presently used to control PM and IM machines for automotive applications. However, some method is needed to drive an appropriate field winding current. To create the field current, it is proposed that the three motor phases be terminated into a three-phase rectifier bridge to drive the field winding, as shown notionally in Figure 2. The output of the rectifier is connected to the field winding, producing a DC current in the field winding that has approximately the same magnitude as the phase current amplitude. No additional active electronics are needed to supply field current. Because the field winding is connected in series with the phase currents via a rectifier, the configuration is deemed "series-wound", notionally similar to the way in which the field is driven in a series-wound DC motor (or series commutator motor in [7]).

Because the field is driven by the phase currents, there is a fixed relationship between the phase current amplitude and the field current. The number of turns in the field winding must be carefully selected so that good performance, particularly with respect to power factor, can be obtained. To select a reasonable number of turns, the case can be considered where stator resistance and leakage inductance are negligible. To simplify the analysis, a version of the field current scaled by the ratio of the phase turns per coil to the field turns per coil is defined as:

$$I_f = c\, i_f \tag{2}$$

where c is the ratio of phase coil turns to field coil turns. With this field current scaling, (1) simplifies to:

$$j\omega Li = v - j\omega LI_f \tag{3}$$

Phase current i is can be decomposed into direct and quadrature components as:

$$i = i_d + j\, i_q \tag{4}$$

The per-phase real power, P, can then be written as:

$$P = \frac{1}{2}\omega LI_f i_q \tag{5}$$

and the per-phase apparent power, S, is:

$$S = \frac{1}{2}L\sqrt{\left(i_d^2 + i_q^2\right)\left(\left(i_d + I_f\right)^2 + i_q^2\right)} \tag{6}$$

Due to the action of the rectifier, the relationship between the field current and the D- and Q-axis currents is fixed:

$$i_f = \sqrt{i_d^2 + i_q^2} \tag{7}$$

The scaled field current, I_f, can be written in terms of the D- and Q- axis currents as:

$$I_f = c\sqrt{i_d^2 + i_q^2} \tag{8}$$

For a particular value of turns ratio c, one can solve for the value of i_d that makes $P = S$ (*i.e.* resulting in unity power factor operation):

$$i_d = -\frac{i_q}{\sqrt{c^2 - 1}} \tag{9}$$

A reasonable choice of c is $c = \sqrt{2}$, which implies that $i_d = i_q$ under unity power factor operation. To obtain this operating point with a three-phase rectifier producing the field current, the number of field turns must be:

$$n_f = c\, n = \sqrt{2}n \tag{10}$$

The specific design shown in Table 1 specifies 10 turns per field coil and 7 turns per phase coil, conforming to this design guideline.

It should be noted that there is some asymmetry in the DSSM configuration because the A and C phases are always on the outside of each three-phase group. Some of this asymmetry is potentially due to different lengths traversed by flux in the stator back iron. This component of the asymmetry can be mitigated by machine designs with adequate back iron thickness, ensuring that heavy saturation occurs in the stator teeth but not in the stator back iron. A back iron thickness of at least 130% of the stator tooth thickness is recommended. A second cause of asymmetry is asymmetric leakage flux couplings between the phases. To obtain balanced, three-phase currents, slightly unbalanced voltages may need to be commanded. The correct voltages can be obtained by implementing a current controller that includes a control for negative sequence as well as positive sequence currents, for example as in [10].

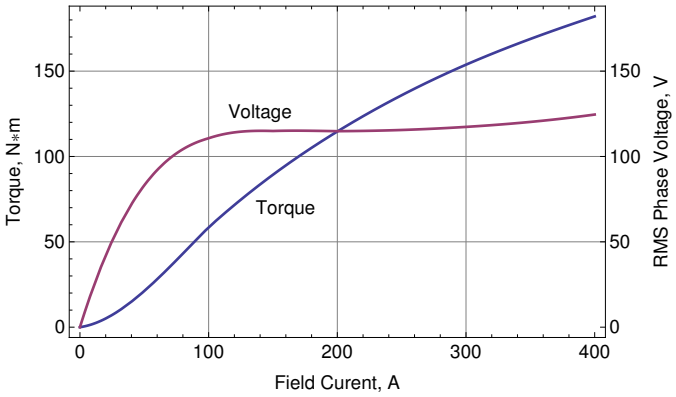

Fig. 3. Phase Voltage versus Field Current for a typical machine (at a 60° phase angle)

III. Proposed Control Approach

Although the DSSM has the same mathematical form as a cylindrical wound-field motor, magnetic saturation and the deterministic relationship between field current amplitude and phase current make the control of the machine novel. Since the field winding current and phase current amplitude are slaved together, the machine can be controlled by selecting the field current (i_f) and phase angle ϕ. These control parameters map onto the commanded currents in the DQ frame using the formulas:

$$\begin{aligned} i_d &= -i_f \cos\phi \\ i_q &= i_f \sin\phi * \mathrm{sgn}(\tau_{des}) \end{aligned} \tag{11}$$

where τ_{des} denotes the desired motor torque. These DQ-frame currents are realized via a standard voltage source inverter running in closed-loop current mode. Note that the negative sign on i_d means that the direct axis current tends buck the flux from the field coils. At the base speed and below, a combination of good power factor and efficiency is achieved by selecting ϕ to be a constant angle of 60° and selecting the field current to be that which is needed to produce the desired torque.

The machine typically runs in a highly saturated regime– finite element analysis is used to map out the relationship between i_f and torque at a constant ϕ. For a typical machine (*e.g.* a machine designed for continuous 50kW operation at a 4000RPM base speed as in [6]), the field current vs. torque graph looks as shown in Figure 3. Note that rather than having a quadratic form (which would be expected in a machine with the materials operating in a linear region), the form of the curve is nearly linear due to a high level of magnetic saturation.

Furthermore, the finite element analysis shows that the required phase voltage is nearly flat versus field current at higher levels of current, as also shown in Figure 3. This form of voltage vs. current implies that the incremental inductance of the machine is low, and that good transient performance might be achieved with the machine.

A window into the behavior of the machine above the base speed (in the field weakening region) can be gleaned by

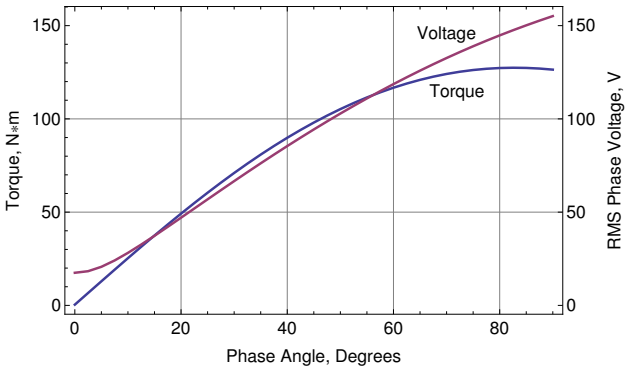

Fig. 4. Torque and Voltage versus Phase Angle at Constant Speed for 200Apk current.

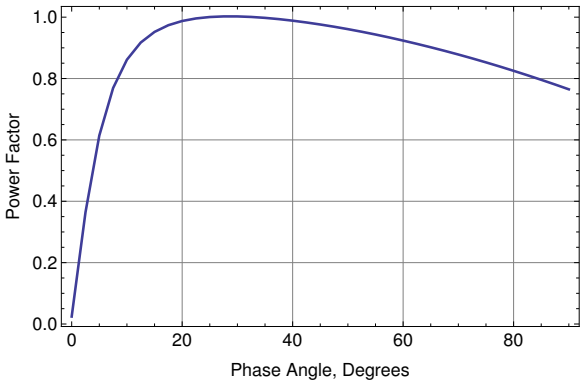

Fig. 5. Power Factor vs. Phase Angle at Constant Speed for 200Apk current.

considering the behavior of the machine at the base current level but at different phase angles. For this specific example, the base current level is taken to be 200A of field current. Figure 4 shows Torque and Voltage versus Phase Angle, ϕ, at the base speed and Figure 5 shows the Power Factor versus Phase Angle.

To control the machine, a method of picking the commanded DQ-frame currents is needed that approximately inverts the graphs shown in Figures 3 and 4. Below the base speed, it is reasonable to pick a constant ϕ and assume that the field current (and therefore i_d and i_q) scales more or less linearly with the desired torque. This assumption approximates the torque curve as a straight line over the range of field current from 0A to 200A. Above the base speed, the phase angle should decrease with increasing speed, walking the power factor from the nominal ($\approx 60°$) operating point to the left over the maximum in power factor and holding voltage largely constant as speed increases. The corresponding reduction in power/voltage allows good field weakening performance up to about 3X the base speed, until the power factor starts to drop unacceptably with further reduction in phase angle ϕ.

An approximate inverse to the machine's performance curves is obtained by first defining the following values:

- τ_o is the "Base Torque". The Base Torque is the maximum continuous torque that can be produced at the machine's nominal operating speed

TABLE II
VECTOR CONTROL PARAMETERS FOR EXAMPLE MACHINE.

Parameter	**Value**
Base Field Current i_{fo}	200A
Base Speed Ω_o	4000 RPM
Base Phase Angle ϕ_o	$62°$
Base Torque τ_o	118.65 N*m
Maximum Phase Angle ϕ_{max}	$62°$
Minimum Phase Angle ϕ_{min}	$10.25°$

- Ω_o is the "Base Speed". The Base Speed is the machine's nominal operating speed and the highest speed that can be achieved without using "field weakening" to accommodate drive voltage.
- i_{fo} is the "Base Field Current". This is the field current that is required to make the Base Torque at the Base Speed.
- ϕ_o is an angle defining the split between D- and Q- axis currents at the Base Torque and Speed.
- ϕ_{max} is the upper bound on the angle defining the split between D- and Q-axis currents. This bound is engaged at or below the Base Speed, and might be equal to ϕ_o.
- ϕ_{min} is the lower bound on the angle defining the split between D- and Q-axis currents. This bound is approached when the machine's speed is high.

At any particular speed, the maximum allowable torque, τ_{lim}, is defined as:

$$\tau_{lim} = \tau_o \min\left(1, \left|\frac{\Omega_o}{\Omega}\right|\right) \tag{12}$$

The expression for τ_{lim} states that the maximum allowable torque should be decrease as the inverse of rotor speed above the base speed and be constant at or below the base speed.

The field current is then prescribed by linearly interpolating from the current required to create the maximum allowable torque at the current speed:

$$i_f = i_{fo}\left|\frac{\tau_{des}}{\tau_{lim}}\right| \tag{13}$$

The phase angle is then selected so that above the base speed, the phase angle drops, reducing both torque and voltage.

$$\phi = \min\left(\phi_{max}, \phi_{min} + (\phi_o - \phi_{min})\left(\frac{\Omega_o}{\Omega}\right)^2\right) \tag{14}$$

For a particular machine, the ϕ_{min} parameter should be carefully selected so that above the base speed, the desired torque is generated and the machine's voltage limits are not exceeded. The $(\Omega_o/\Omega)^2$ form was empirically determined to be a reasonable form. The field current and phase angle from (13) and (14) are then used to prescribe the commanded i_d and i_q currents via (11). For the example machine, a selection of parameters is shown in Table II.

The quality of the current/angle prescription can be assessed by computing commanded i_d and i_q currents and then applying those currents back to the same finite element model used to produce Figures 3-5. Figure 6 shows the results for the

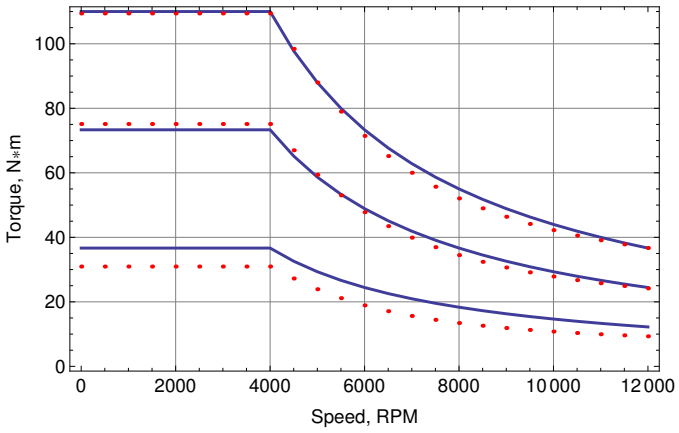

Fig. 6. Commanded torque vs. speed compared to FEA results.

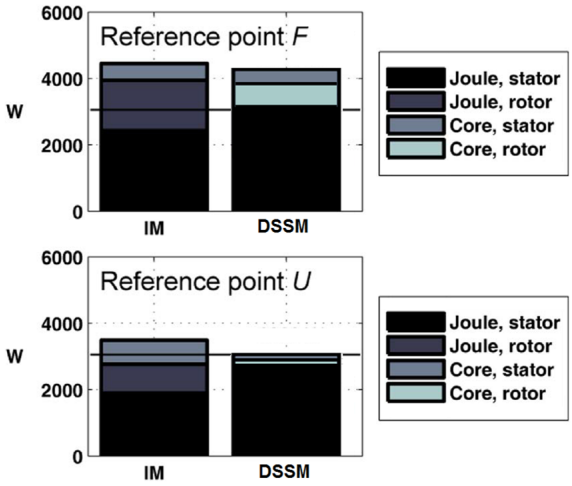

Fig. 7. Losses at 110N*m/4kRPM (U) and 39N*m/12kRPM (F).

110N*m continuous torque from Table I; 2/3 of the continuous torque; and 1/3 of the continuous torque across the full range of operating speeds. The blue line represents the commanded torque at each operating speed, and the points represent the torque computed by applying (13) and (14) to obtain the current command. At high current levels, the match to the commanded torque is good, with an average error of approximately 1.7% for the full torque and 2/3 torque lines. At low commanded torque levels, the error is higher ($\sim 20\%$) because the machine is less saturated and is less well-approximated by a linear relationship between current and torque.

IV. Performance Comparison

In [6], two specific comparison operating points are considered among all machine types: 110 N*m at 4000 RPM (maximum continuous torque at the base speed) and 39 N*m at 12,000 RPM (voltage/current limited operation at the maximum speed). For the DSSM, core losses were computed by the "traditional method" described in [8], by post-processing a series of FEMM [9] 2D magnetostatic finite element simulations performed over one rotation of rotor at 1° increments in rotor mechanical angle. Losses for the IM design are those reported in [6]. The comparison of the losses of the proposed machine versus the IM from [6] is shown below as Figure 7. The (F) operating point considers the example machine operating point of 198Apk at a 16° phase angle, whereas the (U) operating point considers a current of 185Apk at a 62° phase angle.

The total losses from the proposed machine are slightly lower in both cases: 3.2kW vs. 3.5kW at (U) and 4.3kW vs. 4.5kW at (F). Compared to the IM, the DSSM has high stator Joule losses. However, the higher stator losses for the DSSM are a reflection of the fact that both the field and phase coils are on the stator. A better comparison might be to compare total Joule losses in each case–the losses in the proposed machine are slightly less. However, the DSSM has higher rotor core losses. In the DSSM, the rotor iron is exposed to high frequencies, whereas for IMs, the rotor is only exposed to the slip frequency.

It should be noted that relatively conservative fill factors, based on those realized in the existing Proof-of-Concept DSSM described in [4], were assumed. Since most of the losses are resistive, improvements in winding have a dominant effect on overall losses. A better bobbin winding technique may be able to increase fill, thereby further lowering losses.

Because windage losses were not presented in [6], windage loss is not included in Figure 6. Windage losses can be computed for the proposed machine using the technique described in [11]. In [11], windage losses on a toothed rotor are calculated by multiplying a well-known expression for losses on a smooth rotor by an experimentally derived scaling factor. In this case, a scaling factor of 5.95 times the smooth rotor loss was derived from experimentally measured windage loss with an existing machine of a similar geometry [4]. For the geometry in Table I, windage loss is small for at 4,000RPM – approximately 55W. However, the loss increases rapidly with speed, increasing as approximately speed to the 2.73 power. At 12,000 RPM, the calculated windage is 1085W. This windage could be greatly reduced by filling in the gaps between rotor teeth with a non-conductive material, reducing losses to about 182W at 12,000RPM. A mechanically simpler mitigation, as described in [11], is to place a shroud on one end of the rotor, blocking the flow in the space between teeth. The shrouded design is estimated to reduce the windage loses to about 274W at 12,000RPM.

Although detailed predictions of the torque waveform are not available from [6], the torque waveform produced with the proposed machine is still of interest. The torque vs. rotor angle at point (U), as computed via finite element analysis for sinusoidal applied current waveforms, is shown in Figure 8. The ripple of the torque about the steady-state value of 110N*m is about $\pm 2\%$. In comparison, the torque ripple for a similarly sized SRM at a similar torque level [12] is about $\pm 10\%$ using a well-tuned ripple torque reduction strategy or $\pm 30\%$ using a simpler control strategy. The torque ripple at the (F) operating point is shown as Figure 9. The absolute value of the torque ripple is roughly the same as for (U). However,

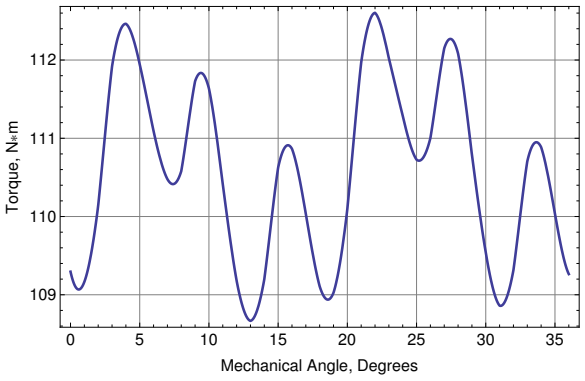

Fig. 8. Torque vs rotor angle for 110N*m/4kRPM (U).

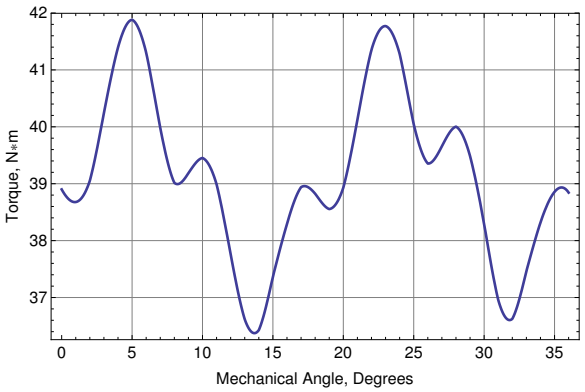

Fig. 9. Torque vs rotor angle for 39N*m/12kRPM (F).

because the torque level is lower, the torque ripple is higher by percentage, here about $\pm 7\%$.

V. Conclusions

A novel heteropolar inductor machine and control approach have been proposed which allow a machine with a simple structure reminiscent of a switched reluctance motor to be driven with a standard voltage source inverter. The volume power density of proposed machine is on a par with an induction machine design of equivalent power rating intended for electric vehicle applications. However, versus induction machines, the proposed machine yields improved power factor and has a simpler structure that may be easier to cool.

A small-scale (15kW) heteropolar inductor machine suitable for a low-power electric vehicle is presently under construction. Future work will present experimental results from the small-scale prototype. Future work could also compare performance to a non-rare earth PM machine and/or evaluate loss and efficiency vs. alternate machine types over various standard driving cycles.

References

[1] Y. Wang and Z. Deng, "Analysis and electromagnetic performance and control schemes of electrical excitation flux-switching machine for DC power systems," *IEEE Trans. Energy Convers.*, vol. 27, no. 4, pp. 844-855, Dec 2012.

[2] P. J. McCleer,"Brushless heteropolar inductor machine," U.S. Patent 6,075,302, June 13, 2000.

[3] D. C. Meeker, "Wound field flux switching machine with sinusoidal back electromotive force," U.S. Patent 9,293,952, March 22, 2016.

[4] D. C. Meeker, "Doubly salient synchronous generator for gas turbine engines," in *Electric Machines Technology Symp.* (EMTS 2014), Villanova, PA, May 28-29, 2014.

[5] I. Boldea et al., "Automotive electric propulsion systems with reduced or no permanent magnets: an overview," *IEEE Trans. Ind. Electron.*, vol. 61, no. 10, pp. 5695-5711, Oct. 2014.

[6] G. Pellegrino et al., "Comparison of induction and PM synchronous motor drives for EV applications including design examples," *IEEE Trans. Ind. Appl.*, vol. 48, no. 6, pp. 2322-2332, Nov/Dec 2012.

[7] G. Slemon, *Electric Machines and Drives*. Reading, MA: Addison-Wesley, 1992.

[8] E. Dlala, "Comparision of models for estimating magnetic core losses in electrical machines using the finite-element method," *IEEE Trans. Magn.*, vol. 45, no. 2, pp. 716-725, Feb. 2009.

[9] D. Meeker, *Finite element method magnetics*, Version 4.2 (15Nov2013 build), Available: http://www.femm.info

[10] H. Song and K. Nam, "Dual current control scheme for PWM converter under unbalanced input voltage conditions," *IEEE Trans. Ind. Electron.*, vol. 46, no. 5, pp. 953-959, Oct. 1999.

[11] J. Vranick, "Prediction of windage power loss in alternators," NASA Technical Note D-4849, Oct. 1968.

[12] R. Vrenken *et al.*, "Switched reluctance motor drive for full electric vehicles – part II: practical implementation," *Eighth International Conference and Exhibition on Ecological Vehicles and Renewable Energies*, Monte Carlo, Mar. 27-30, 2013.